Available online at www.sciencedirect.com
SCIENCE DIRECT
Biochemical and Biophysical Research Communications 338 (2005) 973–980
BBRC
www.elsevier.com/locate/ybbrc

Amyloid fibril formation by macrophage migration inhibitory factor ☆

Hilal A. Lashuel [a,*], Bayan Aljabari [b], Einar M. Sigurdsson [c], Christine N. Metz [b], Lin Leng [d], David J.E. Callaway [b,*], Richard Bucala [d]

[a] *Integrative Biosciences Institute, Laboratory of Molecular Neurobiology and Neuroproteomics, Swiss Federal Institute of Technology (EPFL), CH-1015 Lausanne, Switzerland*
[b] *North Shore Long Island Jewish Research Institute, 300 Community Drive, Manhasset, NY, USA*
[c] *New York University, School of Medicine, Departments of Psychiatry and Pathology, 560 First Avenue, New York, NY, USA*
[d] *Yale University School of Medicine, 300 Cedar Street, New Haven, CT, USA*

Received 3 October 2005
Available online 21 October 2005

Abstract

We demonstrate herein that human macrophage migration inhibitory factor (MIF), a pro-inflammatory cytokine expressed in the brain and not previously considered to be amyloidogenic, forms amyloid fibrils similar to those derived from the disease associated amyloidogenic proteins β-amyloid and α-synuclein. Acid denaturing conditions were found to readily induce MIF to undergo amyloid fibril formation. MIF aggregates to form amyloid-like structures with a morphology that is highly dependent on pH. The mechanism of MIF amyloid formation was probed by electron microscopy, turbidity, Thioflavin T binding, circular dichroism spectroscopy, and analytical ultracentrifugation. The fibrillar structures formed by MIF bind Congo red and exhibit the characteristic green birefringence under polarized light. These results are consistent with the notion that amyloid fibril formation is not an exclusive property of a select group of amyloidogenic proteins, and contribute to a better understanding of the factors which govern protein conformational changes and amyloid fibril formation in vivo.

Keywords: Amyloid; Amyloid fibrils; Alzheimer's disease; Acid denaturation; Macrophage; Migration Inhibitory Factor; Cytokine; P53; Apoptosis; Sedimentation velocity; Electron microscopy

Amyloidogenic proteins undergo a conformational change either prior to or coincident with their self-assembly into highly ordered fibrils that have a characteristic cross β-structure [1]. The presence of amyloid fibrils surrounding dead neurons in the brain is a hallmark of certain neurodegenerative conditions, including Alzheimer's disease, Parkinson's disease, and Prion diseases. Amyloid formation in tissues can also be a pathological sequelae of many chronic inflammatory diseases [2,3]. Electron microscopic examination of the amyloid fibrils that form in vivo reveals long and unbranching filaments that are typically 10 nm in diameter. These fibrils often are detected in vivo by their ability to bind to the dye Congo red, which produces a characteristic green birefringence when illuminated by a polarized light source. Approximately 20 human proteins have been demonstrated to form amyloid in vivo, and several of these have been linked by genetic evidence with neurodegeneration and/or organ dysfunction [4]. A comparison of the primary sequence or tertiary structure of the 20 amyloidogenic proteins that occur in vivo has revealed no clear homology. Nevertheless, these amyloidogenic proteins are each capable of forming highly ordered fibrils of similar structure as discerned by X-ray fibril diffraction, electron, and atomic force microscopy [5]. The ability of these structurally and functionally diverse proteins to form amyloid fibrils with a common structure [6] is puzzling, and has been explained by the apparent tendency of these proteins to adopt a common, alternative β-sheet rich conformation (amyloidogenic intermediate(s)) that facilitates conversion into a cross-β amyloid structure

☆ Supported by NIH Grant 2R01-AI042310-09 (LL, RB).
* Corresponding author. Fax: +41 21 693 17 80.
E-mail address: hilal.lashuel@epfl.ch (H.A. Lashuel).

0006-291X/$ - see front matter © 2005 Elsevier Inc. All rights reserved.
doi:10.1016/j.bbrc.2005.10.040

[4,7]. In the case of the "structured" amyloidogenic proteins transthyretin [8] and lysozyme [9] for instance, the formation of amyloidogenic intermediate(s) has been shown to occur via partial denaturation of the native protein. In the case of "unstructured" amyloidogenic proteins such as β-amyloid, and α-synuclein, amyloid fibril formation appears to proceed via partial folding and linked self-assembly [7]. Recent evidence that several non-amyloidogenic proteins can convert into amyloid under the appropriate conditions nevertheless suggests that amyloid fibril formation is a generic property of many proteins [3,4].

Macrophage migration inhibitory factor (MIF) is a pro-inflammatory cytokine that is highly expressed in many tissues and disease states [10]. Its cellular actions include glucocorticoid counter-regulation [11], sustained MAP kinase activation [12], inhibition of p53-dependent growth arrest [13,14], and control of Jab1 transcriptional effects [15]. There is a significant level of baseline MIF expression in the neurons of the hippocampus as well as in other regions of the brain, and pro-inflammatory stimuli lead to a marked upregulation of neuronal MIF mRNA and protein [16]. MIF's function in the brain is not understood, but its intrinsic tautomerase activity has suggested a possible role in the detoxification of oxidized catecholamines [17]. Interestingly, MIF also has been isolated in association with the Alzheimer's disease, β-amyloid protein [18], which is the main constituent of the fibrils in Alzheimer's disease plaques, thereby supporting an emerging theory of a pro-inflammatory etiology for this neurodegenerative disease.

Human MIF is encoded by a unique gene, and its three-dimensional crystal structure is that of a homotrimer. Each monomer consists of 114 amino acid residues and has a molecular weight of 12,343 Da. As revealed by X-ray crystallography [19,20], the tertiary structure of MIF defines a novel protein fold, which is characterized by the packing of an extended 4-stranded β-sheet and two antiparallel α-helices (Fig. 1A). Three subunits interact via contacts between the β-sheets and wrap completely around to form a symmetrical trimer of a unique α/β structure with a solvent-exposed central channel (Fig. 1B). Although MIF crystallizes as a trimer [19], experimental studies employing NMR spectroscopy [21], size-exclusion chromatography [22], chemical cross-linking [23,24], and analytical ultracentrifugation support the existence of dimeric and monomeric forms in solution [24].

We have observed that partial acid denaturation of recombinant MIF is sufficient to induce amyloid fibril formation. We considered that investigation of the mechanism by which MIF converts from its normally folded, solution form into amyloid fibrils may contribute to a better understanding of the factors which govern protein conformational changes and amyloid fibril formation in vivo. A closer definition of the physicochemical properties of MIF also adds to our comprehension of this mediator's role in immunopathology and neurodegenerative processes.

Material and methods

Protein expression and purification. Recombinant human MIF was expressed in *Escherichia coli* and purified to homogeneity by two successive chromatographic steps as described previously [25]. Buffers used for acid denaturation were 0.05 M phosphate, 0.05 M acetate, and 0.05 M glycine/HCl in the presence of 0.15 M NaCl.

Evaluating secondary structural changes by far-UV circular dichroism. Circular dichroism (CD) spectroscopy was used to evaluate the secondary structural requirements for MIF amyloid fibril formation. The far-UV CD spectra of MIF as a function of pH were recorded on an Aviv Model SF202 spectrometer (25 °C). MIF solutions at a concentration where aggregation does not occur (0.1 and 0.02 mg/mL) and at the desired pH (50 mM acetate or phosphate buffer, 100 mM NaCl) were prepared by dilution of a 0.7–1.0 mg/mL stock solution (10 mM phosphate, 100 mM KCl, and 1 mM EDTA). The CD studies carried out at 0.02 and 0.1 mg/mL were performed using 0.1 cm quartz cuvettes. A step size of 0.2 nm, an averaging time of 3 s, and an average of 15 scans were recorded to generate the data reported in units of mean residue ellipticity. The far- and near-UV CD data were smoothed using a Stineman function (KalidaGraph software), which reduced the noise without perturbing the data.

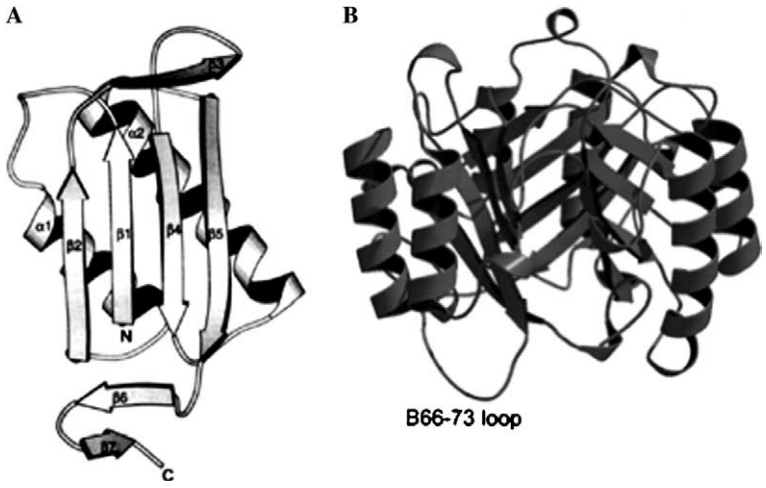

Fig. 1. Ribbon diagram of human macrophage migration inhibitory factor (MIF) monomer (A), and trimer (B).

Evaluating quaternary structural changes by analytical ultracentrifugation. Sedimentation velocity analytical ultracentrifugation experiments were performed to monitor changes in the quaternary structure of MIF during acid-induced denaturation/amyloid fibril formation. Sedimentation velocity experiments were carried out using 400–410 μL of protein solution (0.1–0.3 mg/mL), and data were recorded at rotor speeds of 3000–50,000 rpm in continuous mode at 25 °C with a step size of 0.005 cm. The sedimentation velocity absorbance profiles then were analyzed by fitting the absorbance data using the direct boundary fitting approach or by the time derivative (dc/dt) method to obtain the apparent distribution of sedimentation coefficients g(s*) for all the quaternary structures in solution using the DCDT analysis programs described previously [26].

Aggregation assays. Amyloid formation by MIF as a function of pH was probed using a combination of turbidity and Thioflavin binding assays. For Thioflavin T binding, 29 μL of 0.2 mg/mL solutions of MIF in the appropriate incubation buffer was added to a solution of 10 μL of 100 μM ThT+61 μL of 90 mM glycine–NaOH (pH 8.5 at 25 °C) and ThT fluorescence was measured at $\lambda_{emission} = 482$ nm ($\lambda_{excitation} = 450$ nm).

Congo red birefringence. Drops of fibril-containing solutions were air-dried on gelatin-coated slides. Fibrils produced in vitro by incubation of β-amyloid (Alzheimer's amyloid protein) were used as a positive control. The procedure for Congo red staining of the samples was adapted from that given in [27]. The slides were incubated for 15 min in 80% (v/v) ethanol containing 2% (w/v) Congo red. This was followed by a single wash with saturated lithium carbonate solution and rinsing with distilled water. The slides then were washed in 100% ethanol three times and allowed to dry before being examined between cross-polarizers on a Nikon BN2 microscope.

Electron microscopy. Samples for electron microscopy (EM) were prepared by placing 5 μL of the sample on a glow-discharged carbon-coated grid and allowing the solution to stand for 2 min before removing excess solution. The grid then was washed once with distilled water and once with 1% uranyl acetate before staining the sample with fresh 1% uranyl acetate for another 2 min. The samples were studied with a Phillips CM-100 electron microscope. All electron micrographs were taken at 100 kV.

Tissue preparation and histology. Transgenic mice for the human amyloid precursor protein containing the Swedish mutation (Tg2576) and their wild-type littermates were anesthetized with sodium pentobarbital (150 mg/kg, intraperitoneally) and perfused transaortically with 0.1 M sodium/potassium phosphate buffer (PB, pH 7.4), followed by 4% paraformaldehyde in PB at room temperature. Immediately after beginning the perfusion, 1.0 U/g heparin (Upjohn, Kalamazoo, MI) was administered transaortically. Following perfusion the brain was placed in the fixative for 2 h, and then transferred to a solution containing 20% glycerol and 2% dimethyl sulfoxide dissolved in 0.1 M sodium phosphate buffer, and stored at 4 °C until it was sectioned. Serial coronal sections (40 μm) were cut and every fifth section was stained with IIID9, a mouse monoclonal antibody against mouse [28]. The proinflammatory mediator macrophage migration inhibitory factor (MIF) induces glucose catabolism in muscle. J. Clin. Invest. 106:1291–1300. Adjacent series was stained with 6E10, a mouse monoclonal antibody that selectively binds to human Aβ and stains both pre-amyloid and Aβ plaques [29]. Staining was performed according to a protocol in a mouse-on-mouse (MOM) peroxidase-based immunodetection kit (Vector Laboratories, Burlingame, CA). Briefly, following pretreatment, sections were incubated in: (1) 6E10 (kindly provided by Richard Kascsak, Institute for Basic Research) at a 1:1000 dilution; or (2) IIID9 at a 1:600 dilution. The biotinylated anti-mouse IgG secondary antibody as well as the avidin and peroxidase were used at a 1:2000 dilution. The sections were reacted in 3,3′-diaminobenzidine tetrahydrochloride (Sigma, St. Louis, MO) with nickel ammonium sulfate (Ni; Mallinckrodt, Paris, KY) intensification. Subsequently, the tissue was mounted on slides, dried, defatted, and coverslipped. Staining was also performed on paraffin embedded pre-mounted sections from the temporal cortex of a patient with Alzheimer's disease, with confirmed Aβ plaque deposition. Following deparaffinization, these sections were stained in a similar manner as the mouse sections but the composition of the primary antibody diluent was as described [30]. Some of these sections were pretreated with formic acid and subsequently incubated in the primary antibody overnight at 4 °C. In control mouse and human sections, the primary antibody was omitted.

Results

Since the initial cloning and expression of recombinant MIF by our laboratory, it was noticed that purified MIF has a high tendency to aggregate despite storage under physiological conditions. MIF aggregation was observed to be time- and concentration-dependent, and consequently MIF is usually stored at low solution concentrations (<1 mg/mL), or as a lyophilized powder. MIF's unusual structural properties (an oligomeric α/β protein), and recent reports demonstrating amyloid fibril formation by apparently non-amyloidogenic proteins prompted us to investigate whether the MIF aggregates comprised amyloid fibrils. For most structured proteins (amyloidogenic and non-amyloidogenic), amyloid fibril formation requires a conformational change(s) to produce an aggregation prone intermediate(s) which then self-assembles into amyloid fibrils. Manipulation of protein solution conditions such as pH and temperature typically has been used to induce conformational changes that can promote amyloid fibril. Because native MIF is an oligomeric protein, we considered that partial denaturation of the oligomeric protein and/or dissociation to monomer may be necessary to create a non-native intermediate(s) capable of initiating amyloid fibril formation.

Protofibrils and fibril formation by MIF is pH-dependent and low pH favors fibril formation

Partial denaturation under acidic conditions has been shown to be sufficient to induce amyloid fibril formation by several proteins including those that are not implicated in amyloid diseases [8,31–33]. To determine whether acid-mediated denaturation of MIF is sufficient to induce amyloid fibril formation, we incubated recombinant MIF (0.1 mg/mL) at different pHs (9, 7, 6, 5, 4, 3, and 2) in appropriate buffers (see Material and methods) and in the presence of 0.15 M NaCl for 48–72 h at 37 °C. Employing a stagnant solution, the extent of MIF aggregation as a function of pH was evaluated by monitoring turbidity (330 or 405 nm), ThT binding, and electron microscopy analyses. Both turbidity and ThT measurements clearly show that MIF exhibited maximal aggregation and amyloid formation at a pH of 2–3 (Fig. 2). After 48 of incubation, solutions of MIF also exhibited some turbidity in the pH range of 6–9, however, these aggregates did not bind strongly to ThT, suggesting the formation of amorphous non-amyloid like aggregates. Over the pH range of 4–5 MIF does not aggregate or it aggregates into high molecular weight soluble oligomers that do not bind strongly to ThT.

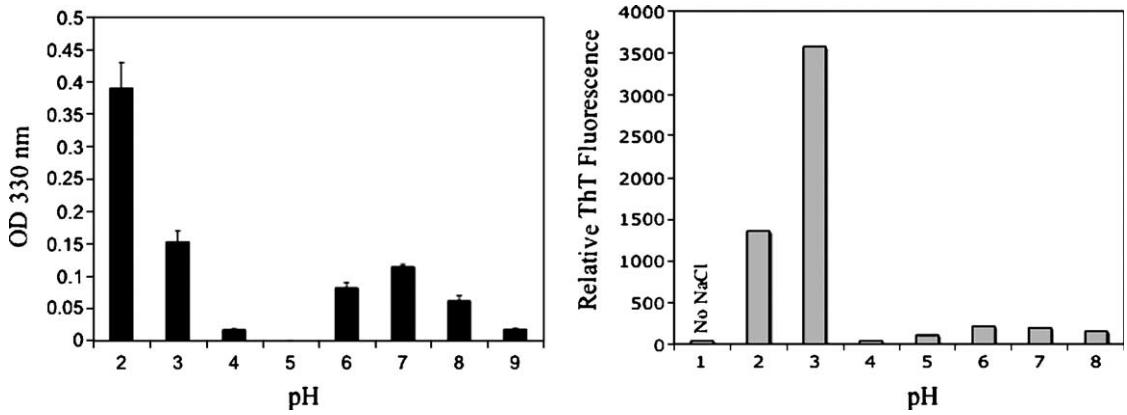

Fig. 2. Bar graph depicting the extent of MIF aggregation as determined by turbidity at 330 nm after 48 h as a function of pH.

Electron microscopy studies

To obtain more information regarding the nature of the acid-induced MIF aggregates, MIF samples (0.1 mg/mL) were incubated at 37 °C for 3 days and studied by electron microscopy. Negatively stained electron micrographs revealed the MIF aggregates to form amyloid-like structures with a morphology that was highly dependent on pH (Fig. 3). In the pH range of 6–8, MIF formed long filaments with an average diameter or 11 nm. Some amorphous aggregates also were present (Fig. 3A). Interestingly, short protofibril-like structures were the dominant species at pH 4 and 5 (Figs. 3B and C). In accordance with the visible absorbance measurements described above, these structures would not be expected to show solution turbidity or strong ThT binding. At pH 2 and 3, extensive formation of amyloid fibrils was observed (Fig. 3D). Long helical filaments with an average diameter of 10 nm were the main species detected, consistent with the maximal turbidity observed at pH 2. Protofibrillar structures were absent at these pHs (2–3).

Congo red binding studies

To further investigate the amyloidogenic nature of the fibrillar structures, the MIF aggregates formed at different

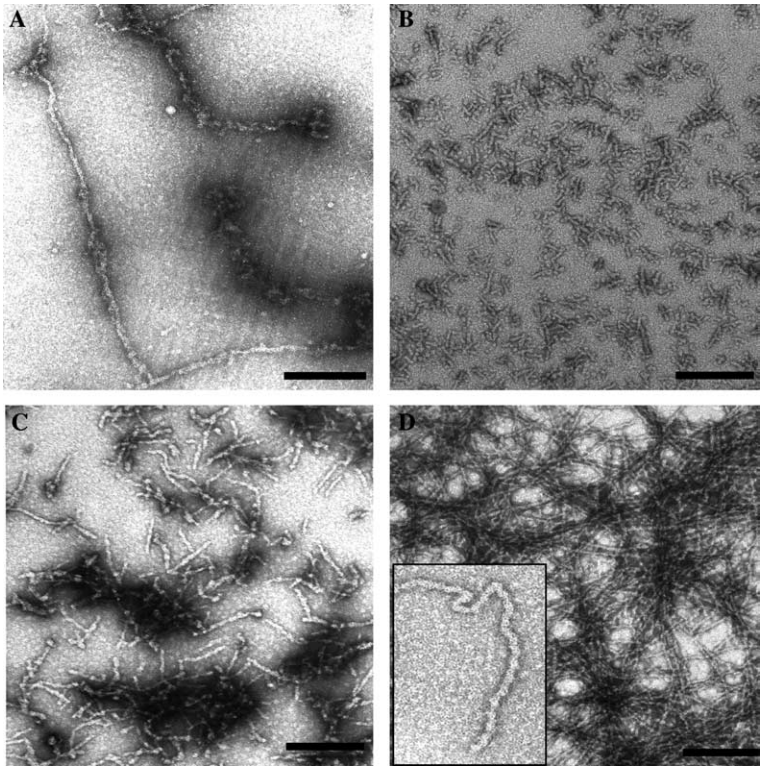

Fig. 3. MIF aggregates to form amyloid-like structures with a morphology that was highly dependent on pH. Negatively stained electron micrographs of MIF after incubation at 37 °C (72 h) at pH 7 (A), pH 4 (B), pH 5 (C), and pH 2 (D). The scale bar represent 100 nm.

pH conditions were examined for their ability to bind the amyloid specific dye Congo red. Congo red is a small organic dye that binds with high affinity to amyloid fibrils, and this interaction results in a characteristic green birefringence when viewed by polarized light microscopy. Both MIF protofibril-like structures (formed at pH 4–5) and amyloid fibrils (formed at pH 2.0) bound Congo red and displayed amyloid-specific green birefringence (Fig. 4). We can not exclude the possibility that these protofibril-like structures could convert to amyloid fibrils during the drying procedure and preparing the sample for Congo red birefringence.

Analytical ultracentrifugation analysis of the pH-dependent quaternary structural changes of MIF

There is some controversy regarding the native oligomeric state of MIF despite the availability of X-ray and NMR structure data for MIF and for MIF complexed with different ligands [34,35]. X-ray crystallography studies indicate that MIF exists predominantly in a trimeric form [36,37], whereas NMR [21], sedimentation velocity [24], size exclusion chromatography [22], and solution cross-linking studies [23] indicate that MIF also may exist in dimeric and monomeric forms. However, recent studies reexamining the molecular size and hydrodynamic properties of MIF in solution suggest that it exists in solution predominantly (>95%) as a trimer, which sediments with a sedimentation coefficient of 3.1S [38].

To study changes in the quaternary structure of MIF induced by acid denaturation and amyloid fibril formation, we used sedimentation velocity analytical ultracentrifugation. For these studies, the MIF solutions were incubated at room temperature for 4–7 h at 25 °C instead of 37 °C so as to minimize protein aggregation. Over the pH range of 9–3, MIF (0.1–0.3 mg/mL) sediments predominantly (96%) as a single species with an s value of 3.1S (±0.1S), consistent with that reported by Philo et al. [38] (Fig. 5A). The sedimentation velocity data also revealed the presence of a second species with an average s value of 5.3, which suggests the presence of a small amount (<5%) of high MW oligomeric species, consistent with previous observations [38]. At pHs ⩽ 3 sedimentation velocity analysis revealed the presence of two species ($s_1 = 2.9$, S 68%, $s_2 = 1.1$ S 32%), suggesting that significant dissociation to the monomer occurs at these pHs. A similar sedimentation coefficient value has been reported for monomeric MIF [38].

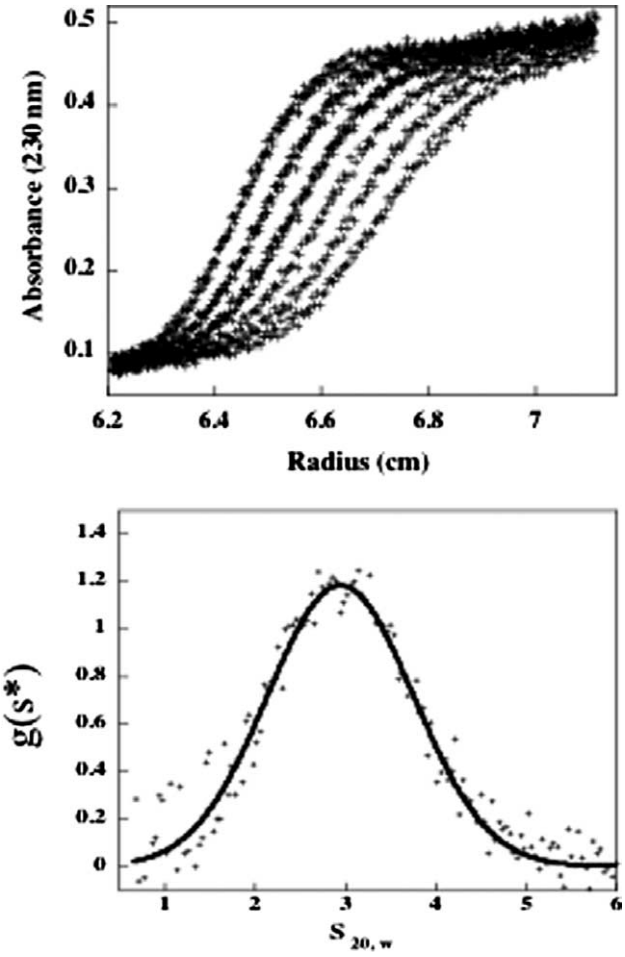

Fig. 5. Sedimentation velocity profiles of MIF (0.1 mg/mL) at pH 7.0 (Overlay of the data sets recorded approximately 10 min apart) and the sedimentation coefficient distribution obtained from analysis of the sedimentation profiles by the dc/dt method.

Far-UV CD of MIF as a function of pH

To further analyze the conformational changes associated with MIF amyloid fibril formation, we conducted

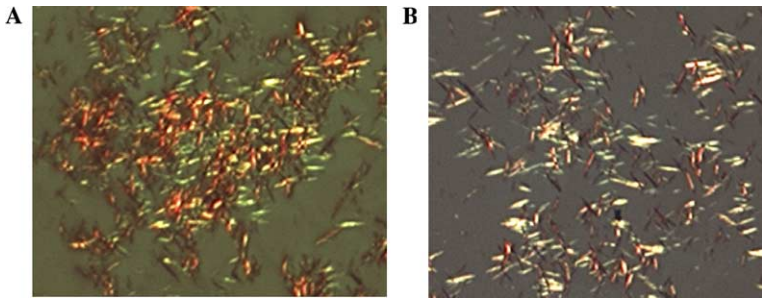

Fig. 4. MIF protofilaments (formed at pH 4–5) and amyloid fibrils (formed at pH 2.0) bound Congo red and displayed amyloid-specific green birefringence. Congo red binding of MIF from an aggregated sample which was incubated (37 °C, 48 h) at pH 4 (A) and pH 2 (B).

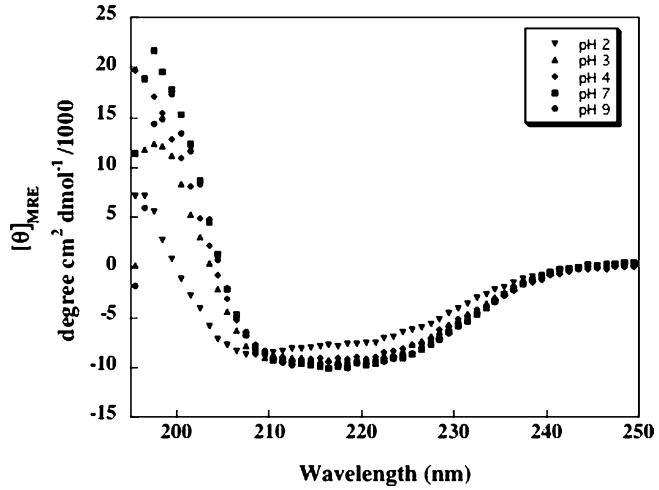

Fig. 6. Far-UV CD spectra of MIF (0.02 mg/mL) as a function of pH.

far-UV CD studies under conditions where aggregation is minimized (0.02 mg/mL, 25 °C). The pH-dependent, far-UV CD spectra of MIF reveals that secondary structural changes during amyloid fibril formation are subtle (Fig. 6). At pH 7 (native conditions), the far-UV CD spectrum of MIF shows a broad minimum between 208 and 220 nm, and a maximum at 197 nm, which is characteristic of a protein composed of mixed α-helical and β-sheet structures. Over the pH range of 9–3, the far-UV CD spectrum did not exhibit any significant changes. Upon lowering the pH 2, the intensity of the minimum and the maximum band decreased significantly, indicating the presence of secondary structural changes associated with the unfolding of the protein. These results suggest that MIF retains most of its secondary structure even at pH 2.0. These observations are consistent with previously reported data [22,39] which suggest that the main structural changes in MIF between pH 7 and 2 are in its tertiary structure.

Discussion

The pro-inflammatory cytokine MIF can be readily induced by acid denaturation to form amyloid fibrils. Circular dichroism measurements clearly demonstrate that MIF is stable over the pH range of 9–4. Furthermore, sedimentation velocity experiments also demonstrate that MIF dissociation does not take place over this pH range, suggesting that a change in tertiary structure may be sufficient to allow for partial rearrangement of the MIF, thereby facilitating MIF self-assembly into high-molecular weight, fibrillar aggregates of different morphologies. Given that the sedimentation velocity experiments were carried out within a few hours of incubation, whereas MIF aggregation was probed after 2–3 days of incubation, we cannot role out the possibility that MIF aggregation goes through a monomeric intermediate under these conditions. The fibrillar aggregates of MIF formed in the pH range of 5–4 were shown to bind Congo red and exhibit the characteristic amyloid green birefringence when viewed under polarized light. Over the pH range of 3–2, MIF begins to undergo dissociation and partial denaturation and exhibits all of the spectroscopic properties of a molten globule A state, which is characterized by the lack of a well-defined tertiary structure. The lack of amyloid formation in the absence of salt at low pHs is consistent with this hypothesis (Fig. 2). Taken together, these data provide a link between the disappearance of tertiary structure and MIF oligomer dissociation, and implicate a molten globule, monomeric MIF species in fibril formation at low pH (3–2). The CD spectrum of MIF at pH 2.0 also demonstrates that MIF does not undergo complete unfolding, but retains significant secondary structure.

Our results are consistent with previously reported data on the acid denaturation of MIF using far, near-UV CD, and fluorescence spectroscopy [22]. These studies showed a pH transition for MIF at a pH of 3.5 ± 0.2. Although MIF did not exhibit any loss in secondary structure over the pH range of 9–4, near UV-CD studies indicate that MIF begins to lose tertiary structure over the pH range of 5–4. Overall, these results clearly support the presence of several structural intermediate(s), including "A state" intermediates, in the acid denaturation pathway for MIF, which are capable of self-assembly into fibrillar aggregates. The morphology of the fibrillar species that form is highly dependent on solution pH, and this is likely due to differences in the tertiary structure of the intermediate that populates a particular pH.

The biophysical and electron microscopy data suggest a scheme for MIF partial denaturation and amyloid fibril formation which is depicted in Fig. 7, where N is native MIF, I is a structured intermediate, A is a molten globule intermediate, and U is the unfolded state of MIF. The circular dichroism studies reported here, as well as elsewhere [22], support the presence of several structured intermediates with variable tertiary structures over the pH range of 5–3. Conceivably, other intermediates not detected by our techniques could be transiently populated at each pH and contribute to fibril formation.

MIF is highly expressed in neurons within different regions of the brain, including the cerebral and cerebellar cortex, the hippocampus, and the hypothalamus. The expression of MIF protein in neuronal tissue is both constitutive and inducible, as revealed by studies of intracisternal endotoxin injection [16]. MIF's precise function in the brain is unknown. MIF-KO mice display no gross central

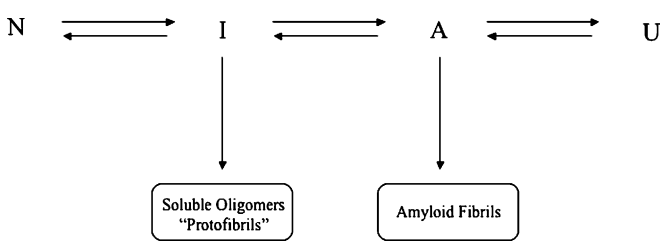

Fig. 7. A schematic depiction of the acid denaturation/amyloid fibril formation pathway of MIF based on the biophysical data presented.

nervous system abnormalities [40,41]; nevertheless, MIF's ability to sustain ERK-1/2 MAP kinase activation and override p53-mediated apoptosis suggests a potentially important role for this protein in neuronal survival [11,12,14]. The recent report of a physical association and co-localization of MIF with the Alzheimer's disease β-amyloid protein combined with the ability of MIF to form amyloid fibrils suggests that MIF may play a role in plaque formation and/or deposition in Alzheimer's disease [18]. However, we failed to observe colocalization of MIF with plaques in the Tg2576 mice or in Alzheimer's brain (*data not shown*). The staining in the mouse brain was similar to MIF staining in rat brain [42]. Immunoreactivity appeared to be primarily located in axons and nerve terminals. Staining in the human brain was more prominent in the formic acid-treated sections and resembled the distribution in the mouse brain. No staining was evident in sections in which the primary antibody was omitted. Further studies are required to investigate the normal function of MIF in the brain and whether it has a potentially pathogenic role in the neuronal cell damage that underlies Alzheimer's neurodegeneration.

Acknowledgments

We are grateful to Drs. J. Lubetsky and E. Lolis for providing the molecular graphic images in Fig. 1.

References

[1] J.W. Kelly, The alternative conformations of amyloidogenic proteins and their multi-step assembly pathways, Curr. Opin. Struct. Biol. 8 (1998) 101–106.
[2] J.C. Rochet, P.T. Lansbury Jr., Amyloid fibrillogenesis: themes and variations, Curr. Opin. Struct. Biol. 10 (2000) 60–68.
[3] M. Stefani, C.M. Dobson, Protein aggregation and aggregate toxicity: new insights into protein folding, misfolding diseases and biological evolution, J. Mol. Med. 81 (2003) 678–699.
[4] C.M. Dobson, Protein folding and misfolding, Nature 426 (2003) 884–890.
[5] M. Sunde, L.C. Serpell, M. Bartlam, P.E. Fraser, M.B. Pepys, C.C. Blake, Common core structure of amyloid fibrils by synchrotron X-ray diffraction, J. Mol. Biol. 273 (1997) 729–739.
[6] B. O'Nuallain, R. Wetzel, Conformational Abs recognizing a generic amyloid fibril epitope, Proc. Natl. Acad. Sci. USA 99 (2002) 1485–1490.
[7] J.W. Kelly, Alternative conformations of amyloidogenic proteins govern their behavior, Curr. Opin. Struct. Biol. 6 (1996) 11–17.
[8] Z. Lai, W. Colon, J.W. Kelly, The acid-mediated denaturation pathway of transthyretin yields a conformational intermediate that can self-assemble into amyloid, Biochemistry 35 (1996) 6470–6482.
[9] D.R. Booth, M. Sunde, V. Bellotti, C.V. Robinson, W.L. Hutchinson, P.E. Fraser, P.N. Hawkins, C.M. Dobson, S.E. Radford, C.C. Blake, M.B. Pepys, Instability, unfolding and aggregation of human lysozyme variants underlying amyloid fibrillogenesis, Nature 385 (1997) 787–793.
[10] C.N. Metz, R. Bucala, Role of macrophage migration inhibitory factor in the regulation of the immune response, Adv. Immunol. 66 (1997) 197–223.
[11] T. Calandra, J. Bernhagen, C.N. Metz, L.A. Spiegel, M. Bacher, T. Donnelly, A. Cerami, R. Bucala, MIF as a glucocorticoid-induced modulator of cytokine production, Nature 377 (1995) 68–71.
[12] R.A. Mitchell, C.N. Metz, T. Peng, R. Bucala, Sustained mitogen-activated protein kinase (MAPK) and cytoplasmic phospholipase A2 activation by macrophage migration inhibitory factor (MIF). Regulatory role in cell proliferation and glucocorticoid action, J. Biol. Chem. 274 (1999) 18100–18106.
[13] J.D. Hudson, M.A. Shoaibi, R. Maestro, A. Carnero, G.J. Hannon, D.H. Beach, A proinflammatory cytokine inhibits p53 tumor suppressor activity, J. Exp. Med. 190 (1999) 1375–1382.
[14] R.A. Mitchell, H. Liao, J. Chesney, G. Fingerle-Rowson, J. Baugh, J. David, R. Bucala, Macrophage migration inhibitory factor (MIF) sustains macrophage proinflammatory function by inhibiting p53: regulatory role in the innate immune response, Proc. Natl. Acad. Sci. USA 99 (2002) 345–350.
[15] R. Kleemann, A. Hausser, G. Geiger, R. Mischke, A. Burger-Kentischer, O. Flieger, F.J. Johannes, T. Roger, T. Calandra, A. Kapurniotu, M. Grell, D. Finkelmeier, H. Brunner, J. Bernhagen, Intracellular action of the cytokine MIF to modulate AP-1 activity and the cell cycle through Jab1, Nature 408 (2000) 211–216.
[16] M. Bacher, A. Meinhardt, H.Y. Lan, F.S. Dhabhar, W. Mu, C.N. Metz, J.A. Chesney, D. Gemsa, T. Donnelly, R.C. Atkins, R. Bucala, MIF expression in the rat brain: implications for neuronal function, Mol. Med. 4 (1998) 217–230.
[17] J. Matsunaga, D. Sinha, L. Pannell, C. Santis, F. Solano, G.J. Wistow, V.J. Hearing, Enzyme activity of macrophage migration inhibitory factor toward oxidized catecholamines, J. Biol. Chem. 274 (1999) 3268–3271.
[18] R. Oyama, H. Yamamoto, K. Titani, Glutamine synthetase, hemoglobin alpha-chain, and macrophage migration inhibitory factor binding to amyloid beta-protein: their identification in rat brain by a novel affinity chromatography and in Alzheimer's disease brain by immunoprecipitation, Biochim. Biophys. Acta 1479 (2000) 91–102.
[19] H.W. Sun, M. Swope, C. Cinquina, S. Bedarkar, J. Bernhagen, R. Bucala, E. Lolis, The subunit structure of human macrophage migration inhibitory factor: evidence for a trimer, Protein Eng. 9 (1996) 631–635.
[20] H. Sugimoto, M. Suzuki, A. Nakagawa, I. Tanaka, M. Fujinaga, J. Nishihira, Crystallization of rat liver macrophage migration inhibitory factor for MAD analysis, J. Struct. Biol. 115 (1995) 331–334.
[21] J. Nishihira, T. Kuriyama, M. Sakai, S. Nishi, S. Ohki, K. Hikichi, The structure and physicochemical properties of rat liver macrophage migration inhibitory factor, Biochim. Biophys. Acta 1247 (1995) 159–162.
[22] E. Zerovnik, V. Janjic, A. Francky, B. Mozetic-Francky, Equilibrium and transient intermediates in folding of human macrophage migration inhibitory factor, Eur. J. Biochem. 260 (1999) 609–618.
[23] R. Mischke, R. Kleemann, H. Brunner, J. Bernhagen, Cross-linking and mutational analysis of the oligomerization state of the cytokine macrophage migration inhibitory factor (MIF), FEBS Lett. 427 (1998) 85–90.
[24] J. Nishihira, T. Kuriyama, H. Nishino, T. Ishibashi, M. Sakai, S. Nishi, Purification and characterization of human macrophage migration inhibitory factor: evidence for specific binding to glutathione and formation of subunit structure, Biochem. Mol. Biol. Int. 31 (1993) 841–850.
[25] J. Bernhagen, R.A. Mitchell, T. Calandra, W. Voelter, A. Cerami, R. Bucala, Purification, bioactivity, and secondary structure analysis of mouse and human macrophage migration inhibitory factor (MIF), Biochemistry 33 (1994) 14144–14155.
[26] W.F. Stafford, Boundary analysis in sedimentation experiments, Methods Enzymol. 240 (1994) 478–501.
[27] G.T. Westermark, K.H. Johnson, P. Westermark, Staining methods for identification of amyloid in tissue, Methods Enzymol. 309 (1999) 3–25.
[28] F. Benigni, T. Atsumi, T. Calandra, C. Metz, B. Echtenacher, T. Peng, R. Bucala, The proinflammatory mediator macrophage migration inhibitory factor induces glucose catabolism in muscle, J. Clin. Invest. 106 (2000) 1291–1300.

[29] K.S. Kim, D.L. Miller, V.J. Sapienza, C.J. Chen, C. Bai, I.G. Iqbal, J.R. Currie, H.M. Wisniewski, Detection and quantification of amyloid β-peptide with 2 monoclonal antibodies, Neurosci. Res. Commun. 7 (1988) 113–122.

[30] E.M. Sigurdsson, S.A. Lorens, M.J. Hejna, X.W. Dong, J.M. Lee, Local and distant histopathological effects of unilateral amyloid-beta 25–35 injections into the amygdala of young F344 rats, Neurobiol. Aging 17 (1996) 893–901.

[31] H.A. Lashuel, C. Wurth, L. Woo, J.W. Kelly, The most pathogenic transthyretin variant, L55P, forms amyloid fibrils under acidic conditions and protofilaments under physiological conditions, Biochemistry 38 (1999) 13560–13573.

[32] F. Chiti, P. Mangione, A. Andreola, S. Giorgetti, M. Stefani, C.M. Dobson, V. Bellotti, N. Taddei, Detection of two partially structured species in the folding process of the amyloidogenic protein beta 2-microglobulin, J. Mol. Biol. 307 (2001) 379–391.

[33] P. Polverino de Laureto, N. Taddei, E. Frare, C. Capanni, S. Costantini, J. Zurdo, F. Chiti Dobson, C.M. Dobson, A. Fontana, Protein aggregation and amyloid fibril formation by an SH3 domain probed by limited proteolysis, J. Mol. Biol. 334 (2003) 129–141.

[34] T. Yoshida, R. Fukatsu, K. Tsuzuki, Y. Aizawa, Y. Hayashi, N. Sasaki, Y. Takamaru, N. Fujii, N. Takahata, Amyloid precursor protein, A beta and amyloid-associated proteins involved in chloroquine retinopathy in rats—immunopathological studies, Brain Res. 764 (1997) 283–288.

[35] A.B. Taylor, W.H. Johnson Jr., R.M. Czerwinski, H.S. Li, M.L. Hackert, C.P. Whitman, Crystal structure of macrophage migration inhibitory factor complexed with (*E*)-2-fluoro-*p*-hydroxycinnamate at 1.8 Å resolution: implications for enzymatic catalysis and inhibition, Biochemistry 38 (1999) 7444–7452.

[36] M. Suzuki, H. Sugimoto, A. Nakagawa, I. Tanaka, J. Nishihira, M. Sakai, Crystal structure of the macrophage migration inhibitory factor from rat liver, Nat. Struct. Biol. 3 (1996) 259–266.

[37] H.W. Sun, J. Bernhagen, R. Bucala, E. Lolis, Crystal structure at 2.6-Å resolution of human macrophage migration inhibitory factor, Proc. Natl. Acad. Sci. USA 93 (1996) 5191–5196.

[38] J.S. Philo, T.H. Yang, M. LaBarre, Re-examining the oligomerization state of macrophage migration inhibitory factor (MIF) in solution, Biophys. Chem. 108 (2004) 77–87.

[39] M.D. Swope, H.W. Sun, B. Klockow, P. Blake, E. Lolis, Macrophage migration inhibitory factor interactions with glutathione and *S*-hexylglutathione, J. Biol. Chem. 273 (1998) 14877–14884.

[40] M. Bozza, A.R. Satoskar, G. Lin, B. Lu, A.A. Humbles, C. Gerard, J.R. David, Targeted disruption of migration inhibitory factor gene reveals its critical role in sepsis, J. Exp. Med. 189 (1999) 341–346.

[41] G. Fingerle-Rowson, O. Petrenko, C.N. Metz, T.G. Forsthuber, R. Mitchell, R. Huss, U. Moll, W. Muller, R. Bucala, The p53-dependent effects of macrophage migration inhibitory factor revealed by gene targeting, Proc. Natl. Acad. Sci. USA 100 (2003) 9354–9359.

[42] M. Bacher, E. Weihe, B. Dietzschold, A. Meinhardt, H. Vedder, D. Gemsa, M. Bette, Borna disease virus-induced accumulation of macrophage migration inhibitory factor in rat brain astrocytes is associated with inhibition of macrophage infiltration, Glia 37 (2002) 291–306.